Structure and dynamics of water surrounding the poly(methacrylic acid): A molecular dynamics study

Shin-Pon Ju[a),b)] and Wen-Jay Lee
Department of Mechanical and Electro-Mechanical Engineering, National Sun-Yat-Sen University, Kaohsiung 804, Taiwan and Center for Nanoscience and Nanotechnology, National Sun-Yat-Sen University, Kaohsiung 804, Taiwan

Ching-I Huang,[a),c)] Wei-Zen Cheng, and Yong-Ting Chung
Institute of Polymer Science and Engineering, National Taiwan University, Taipei 106, Taiwan

(Received 2 March 2007; accepted 4 May 2007; published online 12 June 2007)

All-atom molecular dynamics simulations are used to study a single chain of poly(methacrylic acid) in aqueous solutions at various degrees of charge density. Through a combination of analysis on the radial distribution functions of water and snapshots of the equilibrated structure, we observe that local arrangements of water molecules, surrounding the functional groups of COO^- and COOH in the chain, behave differently and correlated well to the resulting chain conformation behavior. In general, due to strong attractive interactions between water and charged COO^- via the formation of hydrogen bonds, water molecules tend to form shell-like layers around the COO^- groups. Furthermore, water molecules often act as a bridging agent between two neighboring COO^- groups. These bridged water molecules are observed to stabilize the rodlike chain conformation that the highly charged chain reveals, as they significantly limit torsional and bending degrees of the backbone monomers. In addition, they display different dynamic properties from the bulk water. Both the resulting oxygen and hydrogen spectra are greatly shifted due to the presence of strong H-bonded interactions. © *2007 American Institute of Physics*. [DOI: 10.1063/1.2743963]

I. INTRODUCTION

Polyelectrolytes are of great importance due to their extensive presence throughout biological systems and use in a wide range of practical applications, such as sensors, detergents, drug delivery, and gene therapy.[1] In general, polyelectrolytes, when in a solution, dissociate into polyions and counterions. The associated electrostatic interactions that involve the polyions, counterions, and the solvent make the chain conformation behavior of polyelectrolytes quite distinct from that of neutral polymers. Polyelectrolyte conformation has been, and continues to be, an important research area, not only for its relevance to physical properties but also for a deeper understanding of biological phenomena and applications.[1]

Experiments have shown that polyelectrolyte conformation in dilute solutions depends on the charge density that exists along the chain,[2] salt concentration,[2–5] ionic strength,[3] and the solution *p*H value.[6–8] For example, highly charged polyelectrolyte chains in low ionic strength monovalent salt solutions exhibit an extended conformation due to the net repulsion between the charged monomers. When the added salts are multivalent, a series of transitions from extended $\rightarrow$ collapsed $\rightarrow$ reexpanded conformations often occurs upon increasing the salt concentrations. Various theoretical models have shown that the attractive interactions via the associated condensation from multivalent ions along the chains are responsible for the conformational collapse,[3,9–20] whereas the reexpansion of the chains at very high multivalent salt concentrations is mainly attributed to the screening effects of the electrostatic interactions between monomers.[3,10,16,18] Moreover, the degree of reexpansion is strongly related to the overcharge of the polyelectrolytes caused by the condensed ions.[16,19,20] Though current theoretical studies have captured most of the phenomena associated with the conformational variation in polyelectrolytes, solvent effects that involve direct electrostatic interactions between solvent and polyelectrolyte, the local arrangement of the solvent molecules around the polyelectrolyte chain, and the formation of the hydrogen bonds between the solvent molecules and monomers have not yet been addressed. Despite computer simulations that have been employed to study the conformational behavior at an atomistic scale, most related results are based on the so-called coarse grain model.[20–30] To clarify, the solvent is taken into account implicitly as a continuum dielectric with a uniform dielectric constant. We thus employ all-atom molecular dynamics (MD) simulations to study the local structure and dynamics of water in the vicinity of a single polyelectrolyte chain. We show that due to the strong attractive interactions between water and charged monomers, the water molecules form highly bonded structures surrounding the chain via the formation of hydrogen bonds. These bridged water molecules significantly affect the resulting chain conformation behavior as well as their dynamic properties.

[a)]Authors to whom correspondence should be addressed.
[b)]Tel.: 886-7-5252000; Fax: 886-7-5252132; Electronic mail: jushinpon@mail.nsysu.edu.tw
[c)]Tel.: 886-2-33665886; Fax: 886-2-33665237; Electronic mail: chingih@ntu.edu.tw

Water caging behavior has also been noted in a wide range of molecules in aqueous solutions.[31–38] For example, Moelbert *et al.* demonstrated that the micelle formation of small amphiphilic molecules in water is mainly associated with the alteration of water arrangements in the vicinity of the hydrophobic surface regions, driven by the solvent-induced hydrophobic interaction.[32] Solis *et al.* addressed water caging effects on the resulting phase behavior and the calorimetric properties of a lower critical solution temperature type of a gel-forming polymer in water.[33] Recently, by considering all atoms including the solvent within the MD simulation approach, it has also been revealed that the hydration behavior of solvent has a significant influence on the structure and dynamics of the biological molecules.[34–38] For example, Beck *et al.*[34] examined the structure and dynamics of water hydrating peptides and proteins and reported that the bridging water molecules did indeed stabilize and mediate various molecular conformations, including the crown water motif and main chain-side chain bridges. Dudowicz *et al.*[35] studied the hydration structure of a single molecule of met-enkephalin in an aqueous solution and they observed that individual met-enkephalin atoms exhibit various degrees of hydrophobicity by computing the radial distribution functions for all possible pairs of solute and solvent atoms. Lin *et al.*[38] examined the dynamic and thermodynamic properties of water in polyamidoamine (PAMAM) dendrimers and found that the translational and rotational diffusions of water are strongly related to the PAMAM-water interactions, as well as the spatial confinement inside the dendrimer.

In this paper, we consider a single molecule of syndiotactic poly(methacrylic acid) (PMAA) in an aqueous solution. The fact that PMAA exhibits a *p*H dependence to its molecular conformation, as well as its corresponding properties, makes it useful for industrial and biomedical applications.[39–44] Given that PMAA is a weak polyacid, some of the functional groups of COOH in an aqueous medium dissociate into H^+ and COO^- ions. The PMAA chain thus becomes negatively charged due to these COO^- functional groups. In experiments the variation in charge density of the PMAA chains is often accompanied by varying the solution *p*H values. We artificially vary the number of charged monomers N_C, which are equally distributed along the chain with a degree of polymerization N. We then simulate the single PMAA chain in aqueous solutions at various degrees of charge density via the all-atom molecular dynamics simulations. In the study, we ignore the existence of any type of counterions and simply address the associated effects of high hydrophilic COO^- and less hydrophilic COOH functional groups along the chain on the local arrangement, as well as the dynamic behavior of water. This approximation is plausible since the simulation system is highly diluted to avoid having to consider the counterions explicitly. We first analyze the molecular conformation behavior of PMAA at various values of charge density by calculating the radius of gyration of the PMAA chain. In order to examine water distribution surrounding the PMAA chain, we analyze the radial distribution functions (RDFs) of water molecules with respect to COO^- and COOH functional groups. Finally, the dynamic properties of water, due to the presence of H-bonded interactions, are investigated via the self-velocity autocorrelation function (VACF) and the vibration spectra of water molecules.

II. MODEL AND SIMULATION METHODS

We employ an Energy Calculations and Dynamics (ENCAD) simulation program,[45] which is an all-atom model, to calculate the atomic interaction parameters between the PMAA and the solvent water. The total potential energy function U is given as follows:

$$U = U_{\text{bond}} + U_{\text{bend}} + U_{\text{torsion}} + U_{\text{vdW}} + U_{\text{els}}, \tag{1}$$

where U_{bond}, U_{bend}, and U_{torsion} describe the bonded interactions contributed from bond stretching, bond angle bending, and torsion angle twisting, respectively, with the remaining two terms, U_{vdW} and U_{els} representing van der Waals interactions and electrostatic Coulomb potential energy, respectively. Each term has the following form of

$$U_{\text{bond}} = \sum_{\text{bonds}} K_b^i (b_i - b_0^i)^2, \tag{2a}$$

$$U_{\text{bend}} = \sum_{\text{bond angles}} K_\theta^i (\theta_i - \theta_0^i)^2, \tag{2b}$$

$$U_{\text{torsion}} = \sum_{\text{torsion angles}} K_\varphi^i \{1 - \cos[n^i(\varphi_i - \varphi_0^i)]\}, \tag{2c}$$

$$U_{\text{vdW}} = \sum_{\substack{\text{nonbonded pairs } i \text{ and } j \\ \text{closer than cufoff}}} \left[A_{\text{sc}} \varepsilon^{ij} \left(\frac{r_0^{ij}}{r_{ij}} \right)^{12} - 2\varepsilon^{ij} \left(\frac{r_0^{ij}}{r_{ij}} \right)^6 - S_{\text{vdW}}(r_{ij}) \right], \tag{2d}$$

$$U_{\text{els}} = \sum_{\substack{\text{nonbonded pairs } i \text{ and } j \\ \text{closer than cutoff}}} \left[\frac{q_i q_j}{r_{ij}} - S_{\text{els}}(r_{ij}) \right]. \tag{2e}$$

In Eqs. (2a)–(2c), K_b^i, K_θ^i, and K_φ^i correspond to the force constants of the ith bond stretching, ith bond bending, and ith bond torsion angle twisting, respectively; b_i, θ_i, and φ_i are the ith bond length, bending angle, and torsion angle, respectively, and have the corresponding equilibrium values of b_0^i, θ_0^i, and φ_0^i when energy is at a minimum. The torsion energy term U_{torsion} in Eq. (2c) can represent either true dihedral angles or out-of-plane dihedral angles, and is described by cosine functions with a periodicity n^i and a minimum energy at φ_0^i. In Eq. (2d), van der Waals potential U_{vdW} is represented by Lennard-Jones 6-12 potential, where r_{ij} indicates the distance between the ith and jth atoms, and ε^{ij}, r_0^{ij}, and S_{vdW} correspond to the energy parameter between i and j, the equilibrium distance between i and j, and the shift function that compensate for the truncation of the van der Waals interactions at the cutoff distance, respectively. The parameter A_{sc} is used to compensate for the reduced interaction caused by cutoff and has a value dependent on the cutoff distance. In the present study, the cutoff distance has been specified as 8 Å and A_{sc} is assumed to be 0.84.[46] In the Coulomb elec-

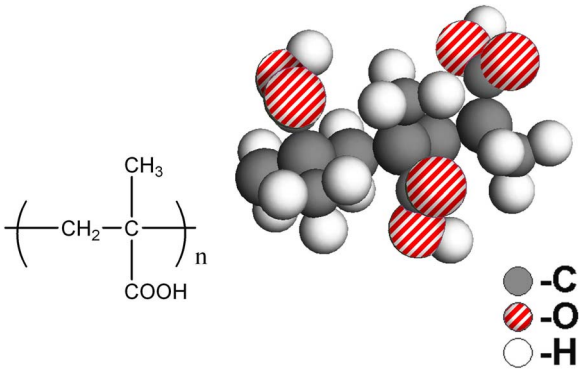

FIG. 1. Schematic representation of PMAA structure.

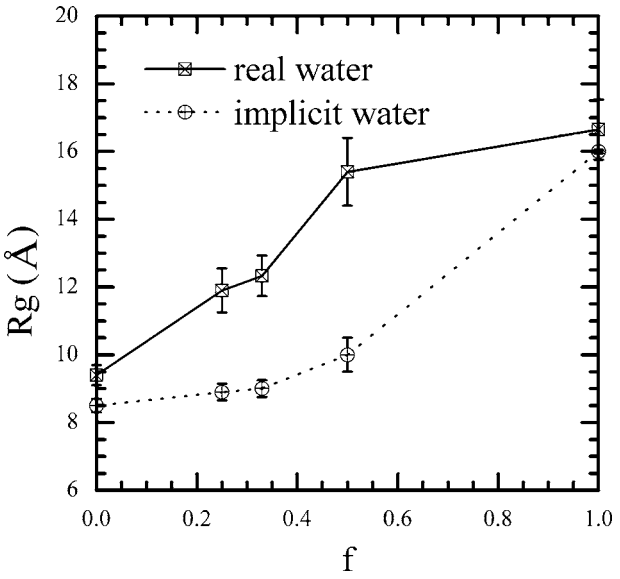

FIG. 2. Plot of the radius of gyration (R_g) of PMAA vs charge density f in the presence of real water and implicit water, respectively.

trostatic potential U_{els} given in Eq. (2e), q^i and q^j represent the partial charges of the ith and jth atoms within the cutoff distance, and S_{els} is the truncation shift function that compensates for the truncation of the electrostatic interactions at the cutoff distance. In Eqs. (2d) and (2e), the potential energy summations are executed over all nonbonded pairs of i and j closer than the cutoff distance. All the parameters of the ENCAD are derived from *ab initio* quantum mechanics, spectroscopy, and crystallography, and can be obtained from Refs. 45 and 46. In addition, the solvent water is treated explicitly via a flexible three-centered (F3C) model, in which the associated water potential still adopts the same type of the force fields as in the ENCAD program.[46] This F3C water model has been proven suitable for describing the structural and dynamic properties of liquid water.

The system contains a single chain of syndiotactic PMAA with a degree of polymerization N equal to 48 in the presence of approximately 1700 water molecules. In our simulations, we used Materials Studio (MS) molecular modeling software to construct the initial atomistic structure of the PMAA, as presented in Fig. 1, and varied the number of charged monomers N_C, which were equally distributed along the chain. In particular, the charge density $f(=N_C/N)$ for the PMAA chain is equal to 1, 0.5, 0.33, 0.25, and 0, respectively. We assumed that no counterions were present in the study. The molecular dynamics simulations were performed by integrating the positions and velocities of all atoms according to the velocity-Verlet algorithm.[47,48] The initial temperature was set at 300 K and the initial velocities of all atoms at 300 K were generated randomly from a Maxwell distribution. The Nosé-Hoover thermostat[47,48] was adopted for temperature control and the integration time step was chosen as 1 fs. The PMAA chain was first put in a vacuum box with a side length of 40 Å and a periodic boundary condition, then the box was gradually filled with water molecules to a density of 0.791 g/cm^3. Prior to simulation, the steepest descent minimization method was adopted to relax and equilibrate the initial structure. To clarify, the PMAA chain was fixed and the water solvent was relaxed to populate the relevant hydration sites on the PMAA for 30 ps in a canonical *NVT* ensemble. This minimized structure was then compressed to a density of 0.987 g/cm^3 at a rate of 0.1 Å/fs, followed by a series of annealing processes. The annealing temperature was first raised from 300 to 600 K at a rate of 5 K/1 ps and kept at 600 K for 100 ps. It was then quenched to 300 K at the same rate and kept at 300 K for 20 ps. This annealing cycle was repeated four to six times to assure that the system had been equilibrated. Finally, it was followed by a long relaxation period of 100 ps at 300 K. After these processes were performed so that the system energy has reached the equilibrium value, we analyzed the radius of gyration (R_g) of the PMAA chain and the (RDF) every 100 fs, as well as the self-VACF of water molecules every 5 fs, which were averaged out for the data collection interval of 10 ps.

III. RESULTS AND DISCUSSION

We begin by examining how the PMAA molecular conformation behavior is affected by the charge density f along the PMAA chain. In general, the molecular conformation behavior of polymer chains is analyzed by calculating the radius of gyration, which is defined as

$$R_g = \langle R_g^2 \rangle = \frac{1}{N} \left\langle \sum_{i=1}^{N} |\mathbf{r}_i - \mathbf{r}_{\text{c.m.}}|^2 \right\rangle, \tag{3}$$

where $\mathbf{r}_i$ and $\mathbf{r}_{\text{c.m.}}$ represent the position vector of the ith atom and the center of mass of the PMAA, respectively. For the same polymer, the larger value of R_g, the more stretched out for the polymer chain. Figure 2 displays the variation in R_g with f, where we also designate the maximum and minimum values of R_g with error bars. In order to clearly manifest the significant effects contributed from real water, we repeat the simulation on the same system; however, the water is treated implicitly as a comparison. To clarify, the solvent is taken into account as a continuum dielectric with a dielectric constant. Consequently, the electrostatic Coulomb interaction term U_{els} becomes $U_{\text{els}}=k_BTl_B\Sigma_{i,j}q_iq_j/r_{ij}$, where l_B is the Bjerrum length and equal to 7 Å in water.[27] Figure 2 clearly shows that with the same charge density f, the value of R_g for the PMAA chain in explicit water is greater than that when the water is treated implicitly. This indicates that the

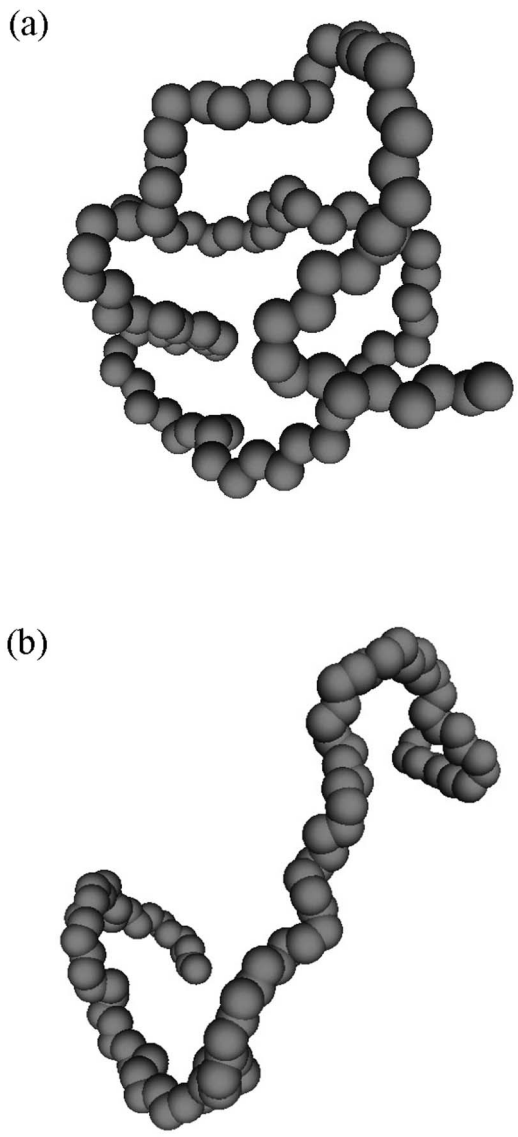

FIG. 3. Snapshots of the equilibrium chain conformation of PMAA with charge density f equal to (a) 0 and (b) 1 in a highly diluted aqueous solution. In each pattern, only the backbone carbon atoms are shown.

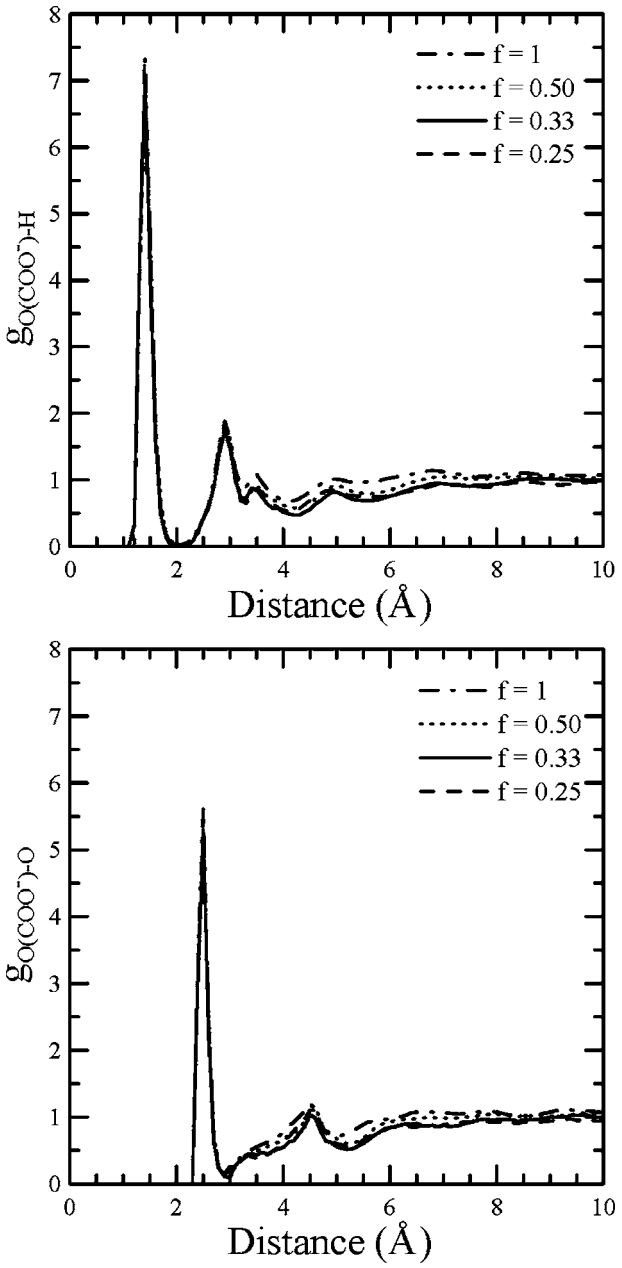

FIG. 4. The radial distribution functions of oxygen (O) and hydrogen (H) atoms of water with respect to the O atom in the COO^- groups at various values of charge density f.

existence of real water causes a greater degree of stretching in the charged polymer chain. As the charge density f increases, due to the fact that the repulsive degree of the electrostatic interactions between the COO^- groups becomes more significant, R_g shows an increasing behavior. Figures 3(a) and 3(b) illustrate the chain conformation of PMAA in a highly diluted aqueous solution at $f=0$ and 1, respectively. When $f=0$, i.e., there exist no electrostatic interactions, the noncharged PMAA chain tends to entangle and forms a coil-like structure, as expected. When $f=1$, i.e., each monomer along the chain is charged, the PMAA chain becomes rodlike except near either end of the chain, which shows a winding structure. This may have been due to the chain at either end having a higher degree of freedom and thus able to fold slightly. Later we will show that the organization of water molecules surrounding the PMAA chain also plays an important role in the PMAA chain conformation behavior.

In aqueous solutions, the hydration behavior of molecules is a complex subject, but worth further exploration. In order to investigate the distribution of water molecules surrounding the PMAA chain, we analyze the radial distribution functions of the oxygen (O) and hydrogen (H) atoms of water with respect to the O atom in the COO^- group, the O atom of carbonyl (–C═O) in the COOH group, and the O atom of hydroxyl (–OH) in the COOH group of the PMAA at various values of charge density f, in Figs. 4–6, respectively, This radial distribution function $g_{A\text{-}B}(r)$ indicates the local probability density of finding B atoms at a distance r from A atoms averaged over the equilibrium density, as follows:

$$g_{A\text{-}B}(r) = \frac{n_B/4\pi r^2 dr}{N_B/V}, \tag{4}$$

where n_B is the number of B atoms at a distance r in a shell of thickness dr from atom A, N_B is the total number of B

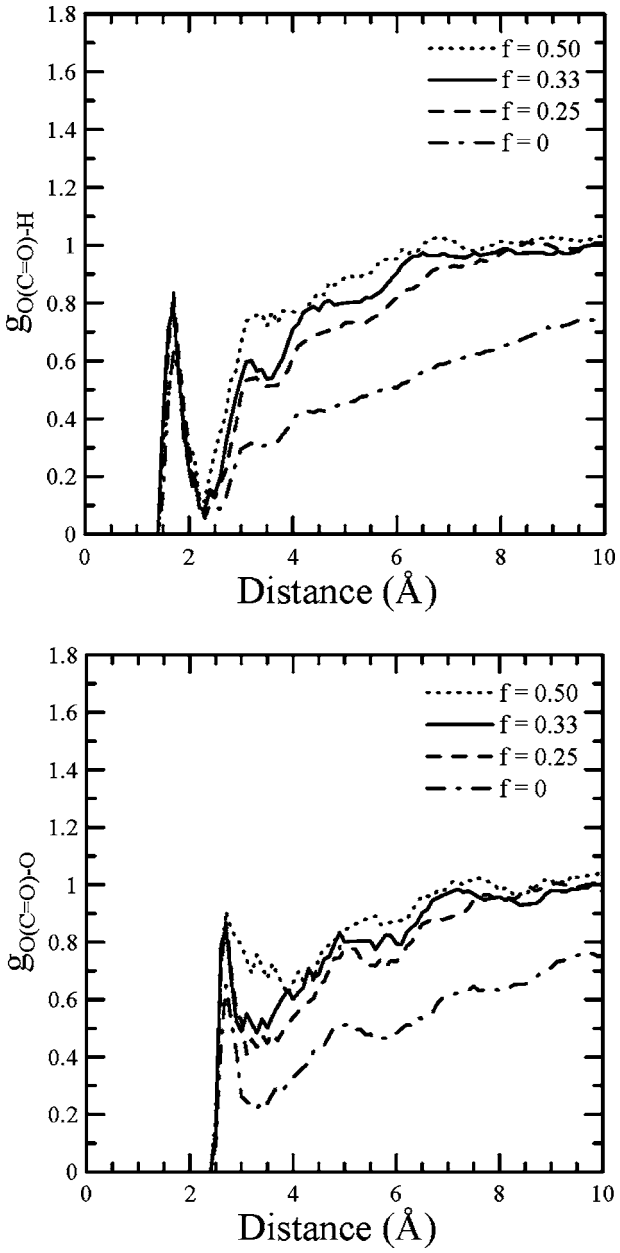

FIG. 5. The radial distribution functions of oxygen (O) and hydrogen (H) atoms of water with respect to the O atom of carbonyl (–C═O) in the COOH groups at various values of charge density f.

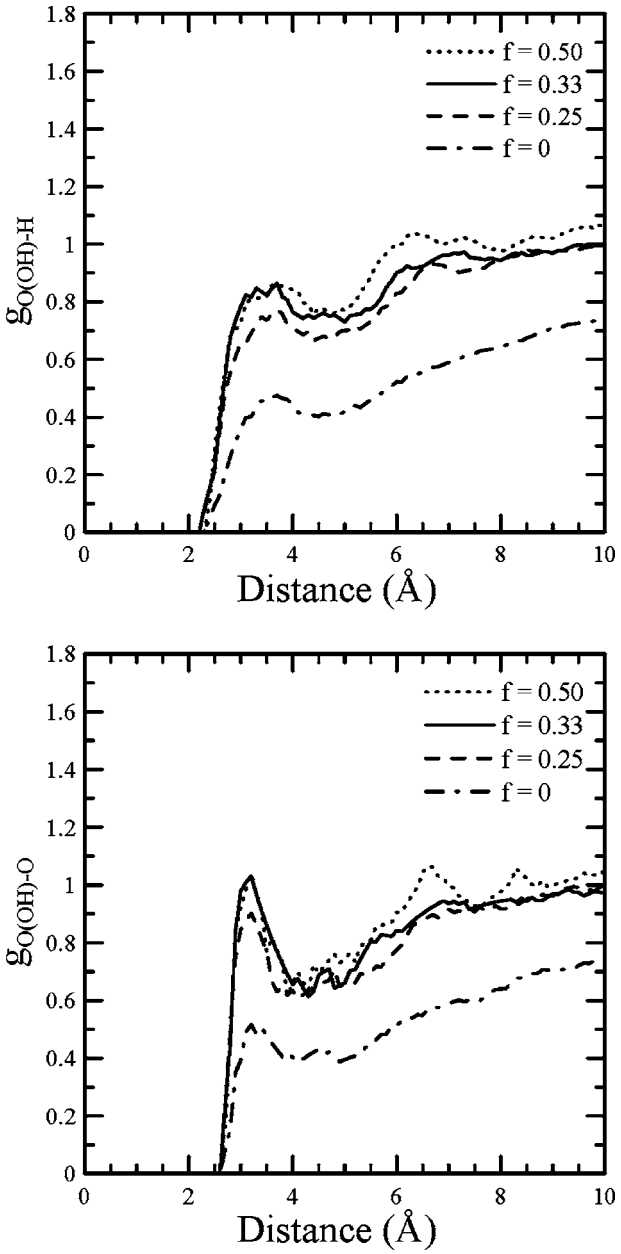

FIG. 6. The radial distribution functions of oxygen (O) and hydrogen (H) atoms of water with respect to the O atom of hydroxyl (–OH) in the COOH groups at various values of charge density f.

atoms in the system, and V is the total volume of the system. In Fig. 4, where the distribution of water (H and O atoms) is analyzed from the central O atom in the COO^- group, we observe two prominent peaks for the hydrogen RDF profiles and one for the oxygen RDF profiles regardless of the charge density f values. These RDF profiles are similar to those obtained from the central O atom of the COO^- group in the met-enkephalin study.[35] The observed high and sharp first peaks as well as the first minimum values close to 0 for both $g_{O(COO^-)-H}$ and $g_{O(COO^-)-O}$ manifest the fact that these COO^- groups are strongly hydrophilic in nature and therefore attract a large amount of water molecules to form shell-like layers surrounding them. In addition, the first peak of the hydrogen RDF profiles occurs at 1.4 Å, which is less than the normal hydrogen bonding length of 1.8 Å,[49] indicating that the interaction between the O atom of the COO^- group and the H atom of the water molecule is stronger than the strength of hydrogen bonds in bulk water. This is expected as polar water molecules and negatively charged oxygen atoms have a stronger interaction than in bulk water.[35] Next, we discuss the distribution of water surrounding the COOH group, as shown in Figs. 5 and 6. When water distribution is analyzed from the central O atom of carbonyl (–C═O) in the COOH group (Fig. 5), each hydrogen and oxygen RDF profile displays a clear peak at 1.7 and 2.7 Å, respectively, at various values of charge density f, which indicates that a shell-like layer of water molecules forms around the O atom in the COOH group. The peak positions are close to those corresponding to hydrogen bonding water molecules in bulk water.[46,49] However, the broad first peaks observed in the H

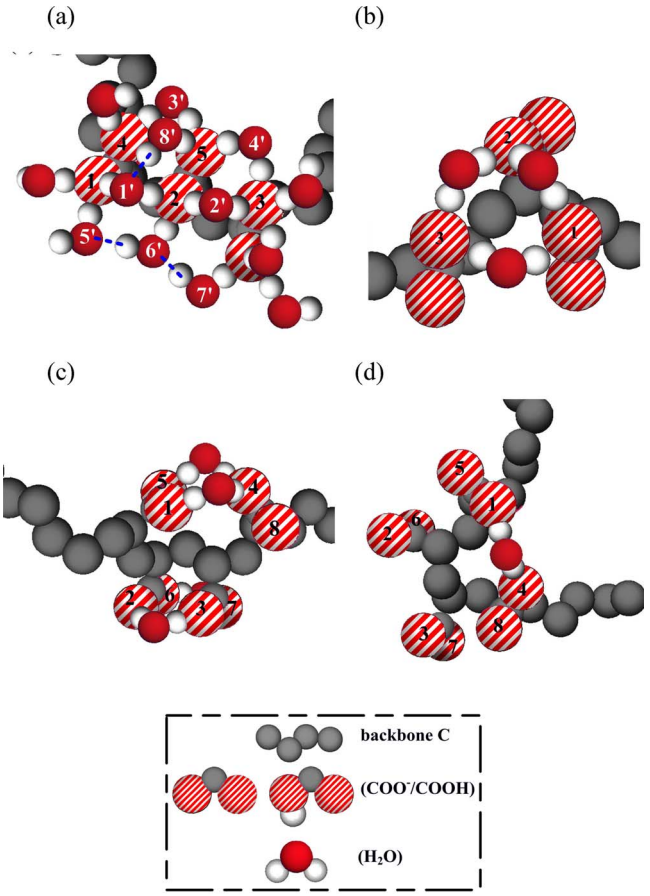

FIG. 7. Snapshots of several characteristic arrangements of water molecules around the three sequential monomers with COO^- side groups, in which the PMAA chain shows a local rodlike structure for (a)–(c) and a winding structure near the ends of the chain for (d). Note, in (b)–(d), we only display the bridged water molecules.

and O distribution profiles in Fig. 6 reveal that water molecules do not distribute closely around the central O atom of hydroxyl (–OH) in the COOH group. Furthermore, we observe that the first peak position for the $g_{O(-OH)-H}$ profile at 3.7 Å is greater than that for the $g_{O(-OH)-O}$ profile at 3.2 Å. This is simply because among the hydroxyl (–OH) in the COOH group the one that forms hydrogen bonds with water molecules is the H atom instead of the O atom. Hence, the probability of finding the O atom of water is greater than that of finding the H atom of water. In addition, the height of the first peaks in both Figs. 5 and 6 is less than 1, i.e., the local water density surrounding the COOH groups is even smaller than that of bulk water. To clarify, only a small amount of hydrogen bonds form between the water molecules and the COOH groups. Indeed, for the noncharged PMAA case ($f=0$), we observe that when the distance from the COOH group is smaller than R_g ($\cong 10$ Å), all the water distribution profiles are far less than 1.0. This indicates that the COOH groups appear to be less hydrophilic in nature and therefore fewer water molecules could remain inside the coiled PMAA chain.

Next, we examine the local arrangements of water molecules surrounding the PMAA chain and their effects on the resulting chain conformation behavior. Figure 7 illustrates several characteristic arrangements of water molecules around the sequential monomers with COO^- side groups, i.e., when the charge density $f=1$. In particular, (a)–(c) demonstrate typical water organization behavior around the local rodlike PMAA chain and (d) displays the water organization behavior near the ends of the chain showing a winding structure. In Fig. 7(a), where the O atoms of three sequential COO^- groups are located on the same side and very nearly arrange in a straight line, it is clear that each O atom is closely surrounded by three water molecules. Surprisingly, each pair of neighboring O atoms of different COO^- groups is strongly bonded to the H atoms of a single water molecule, which acts as a bridging agent. For example, water molecules 1′, 2′, 3′, and 4′ are located between O atoms 1 and 2, 2 and 3, 4 and 5, and 3 and 5, respectively. Moreover, there form the hydrogen bonds between the adsorbed water molecules designated as 5′ and 6′, 6′ and 7′, and 1′ and 8′, respectively. It is reasonable to conclude that these strong bridging interactions via water molecules contribute to forming the stable rodlike chain conformation, as they are able to significantly limit torsional and bending degrees of the backbone monomers. Here we apply geometric measurement to define the location of the hydrogen bonds formed between two molecules, as in Ref. 50: (1) the distance between the O atoms of both molecules is smaller than 3.6 Å; (2) the distance between the hydrogen of the donor molecule and the oxygen of the acceptor is smaller than 2.45 Å; (3) the angle between the O–H bond of the water molecule and O··O of two molecules is smaller than 30°. Note, since we are concerned as to whether the water bridging behavior also occurs in Figs. 7(b)–7(d), we did not present the detailed water arrangement behavior along each COO^- group as in Fig. 7(a), and only described the bridged water molecules. Clearly, similar bridging behavior via water molecules has also been observed in Fig. 7(b), where the O atoms designated as 1, 2, and 3 in the three sequential COO^- groups form a triangle, and each pair of 1-2, 2-3, and 1-3 O atoms are also bonded to a single water molecule, respectively. In addition, Fig. 7(c) shows a third possible water organization behavior along the locally stretched chain. Though the non-neighboring pairs 1-4 and 5-4 O atoms are bridged by water molecules, which may cause the chain to fold slightly, the fact that there also exist water molecules between the neighboring pairs 2-3 and 6-7 O atoms hinders the bending of the polymer chain. While in Fig. 7(d), which is a typical snapshot of local water arrangements near the ends of the chain, we observe no water molecules between the neighboring O atoms. Hence, the bridging behavior via the water between the non-neighboring O atoms leads the tail to form a winding conformation. These observations have revealed that in addition to the repulsive electrostatic interactions between the charged monomers, the local bridging arrangement of water molecules around the O atoms of the COO^- groups also contributes to the stretched or rodlike conformation of the polyelectrolyte chain in aqueous solutions. Note, some of these water molecules that stabilize the stretched molecular conformation remain steady between the COO^- groups for more than 10 ps; while some of the absorbed water molecules may fade away after a period of less than 3.5 ps, which we will discuss in more detail later. When the charge density f is between 0 and

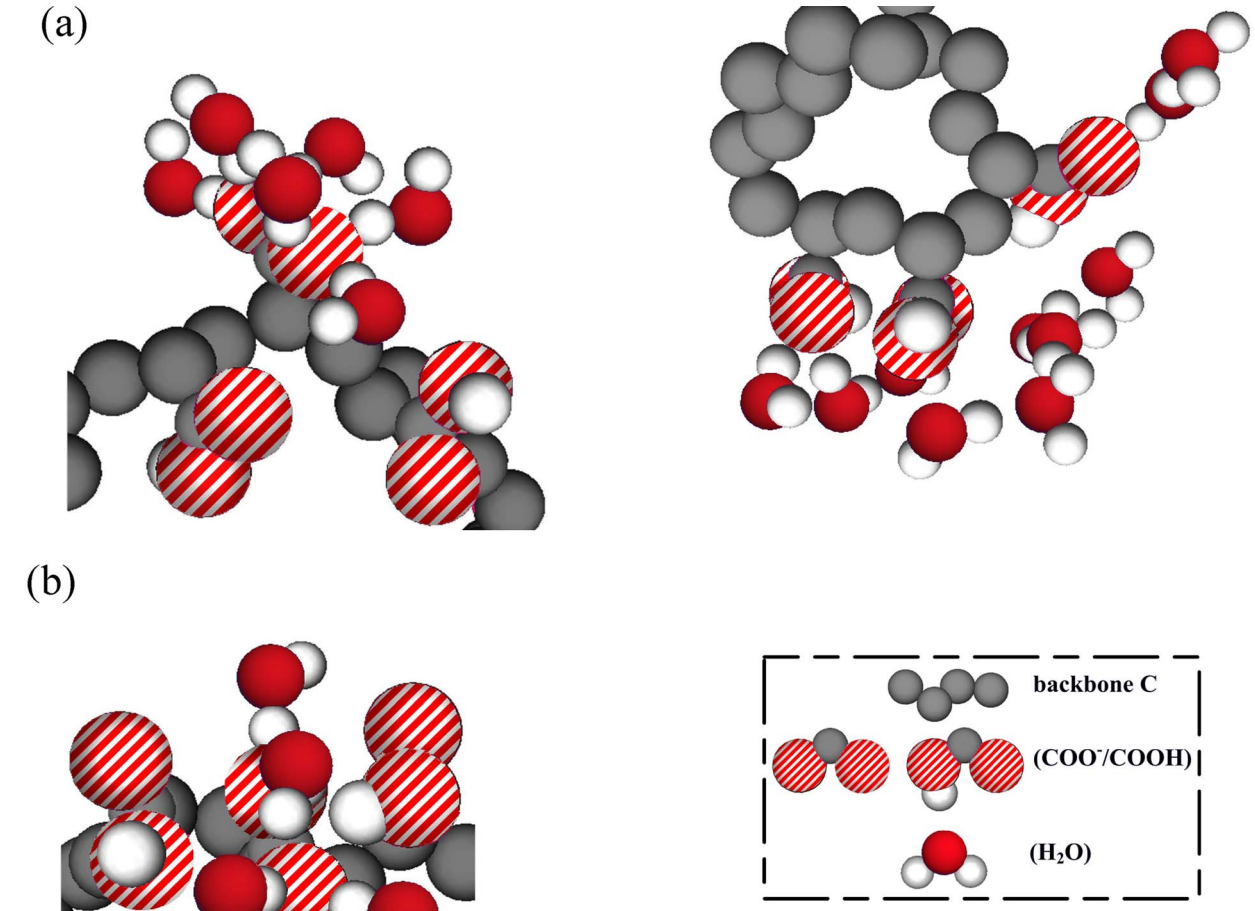

FIG. 8. Snapshots of characteristic arrangements of water molecules around the COO^- functional group in the sequential COOH–COO^-–COOH, in which the two COOH groups and COO^- are located (a) on different sides and (b) on the same side.

FIG. 9. Snapshot of characteristic arrangements of water molecules around the three sequential monomers of COOH groups.

1, the typical arrangement of water molecules around the COO^- functional group in the sequential COOH–COO^-–COOH is displayed in Fig. 8. Note, in particular, that when two COOH and COO^- groups are located on different sides, as presented in Fig. 8(a), each O atom of the COO^- group attracts three water molecules. However, when three sequential COOH–COO^-–COOH groups are on the same side, the nature of the two less hydrophilic COOH groups may prevent the adsorption of water molecules around the COO^- group and thereafter the number of water molecules attracted to the O atom of the COO^- group decreases from 3 to 2, as shown in Fig. 8(b). Regardless of the type of spatial arrangement between the three sequential COOH–COO^-–COOH groups, it is clear that no water molecules bridge between the COO^- and COOH groups, as we frequently observe between the two COO^- groups. When the charge density f decreases to 0, as shown in Fig. 9 where we present the typical water organization behavior around sequential COOH groups, though it is possible for water molecules to form a hydrogen bond with the COOH, most likely they are farther from the COOH group. This supports evidence from the corresponding RDF profiles in Figs. 5 and 6. Hence, these COOH groups can be drawn closer to each other allowing the PMAA chain to form an entangled conformation.

As the RDF profiles, mentioned above, have shown, local distribution of water surrounding the functional groups in the PMAA chain differs from the behavior of bulk water. Consequently, these adsorbed water molecules display significantly different dynamic behaviors. In order to analyze the dynamic properties of water, we first classify the water molecules into three states: bulk water (designated as W0), water with a single H atom hydrogen bonded with the COO^- group (W1), and bridged water with two H atoms bonded with the COO^- groups (W2). Accordingly, we classify the oxygen atoms into three types, O0, O1, and O2, which belong to the water molecule states described above, respectively. Similarly, the hydrogen atoms are divided into four

TABLE I. Fractions of each type of water molecules, W1 and W2, which are stable around the COO^- groups during the data collection interval of 10 ps, and W1′ and W2′, which fade away after 3.5 ps.

Type	Fraction
W1	0.005
W1′	0.065
W2	0.160
W2′	0.040

types of H0, H1y, H1n, and H2. Note, for the water molecules with only one hydrogen bond formed with the COO^- group (i.e., state 1), the two types of hydrogen-bonded and non-hydrogen-bonded H atoms are denoted as H1y and H1n, respectively. Prior to analyzing the dynamic properties of water, we have to examine whether the adsorbed water molecules of W1 and W2 surrounding the COO^- groups are stable by calculating the time dependence of the average mean-squared displacement of adsorbed hydrogen with respect to the oxygen in the COO^- groups,

$$\langle \Delta r^2 \rangle = \langle |\mathbf{r}_{H(W)}(t) - \mathbf{r}_{O(COO^-)}(t)|^2 \rangle, \tag{5}$$

where $\mathbf{r}_{H(W)}(t)$ and $\mathbf{r}_{O(COO^-)}(t)$ correspond to the position vectors of the H atoms in water molecules and the O atoms in the COO^- groups, respectively. In Table I, we list the fractions of each type of water molecules, W1 and W2, which are stable around the COO^- groups during the data collection interval of 10 ps. Also listed are the fractions of W1′ and W2′, which, although initially are adsorbed around the COO^-, fade away after 3.5 ps. Figure 10 presents the resulting plot of $\langle \Delta r^2 \rangle$ vs t for W1, W2, W1′ and W2′. As shown in Table I, there exist very few stable W1 molecules (~0.005); whereas, a significant fraction 0.16 of water molecules are able to steadily bridge between the COO^- functional groups for 10 ps. The existence of these stable bridged water molecules supports one of the main results previously obtained that the rodlike chain conformation for a highly charged chain is indeed significantly enhanced by them.

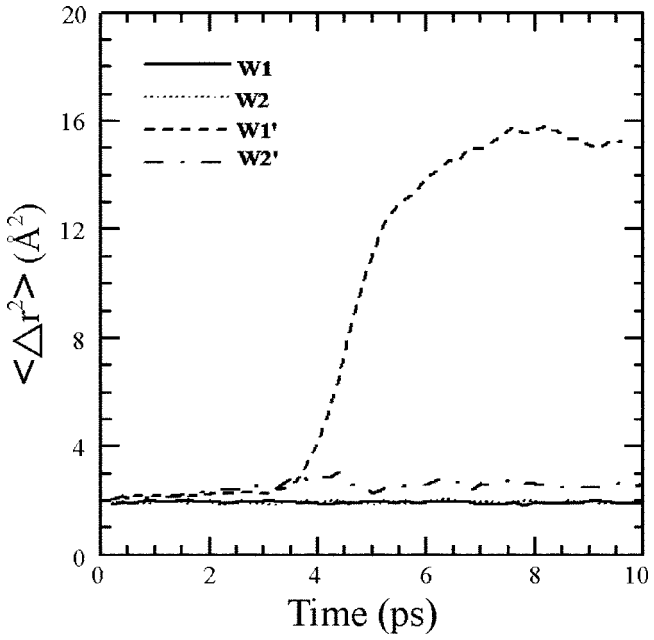

FIG. 10. Plot of mean-squared displacement $\langle \Delta r^2 \rangle$ vs t for the hydrogen atoms which belong to the water molecules W1, W2, W1′, and W2′, respectively, with respect to the oxygen in the COO^- group.

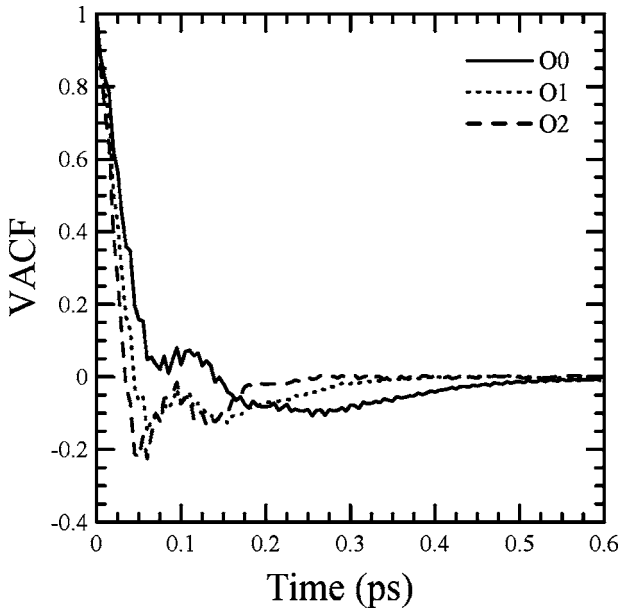

FIG. 11. The self-velocity autocorrelation functions (VACFs) for water oxygen belonging to the water molecules in the bulk state (O0), with a single H atom hydrogen bonded with the COO^- group (O1), and with two H atoms bonded with the COO^- groups (O2), respectively.

Next we calculate the self-velocity autocorrelation function (VACF), as defined by

$$G(\tau) = \frac{\langle \nu_i(t_0) \cdot \nu_i(t_0 + \tau) \rangle}{\langle \nu_i(t_0) \cdot \nu_i(t_0) \rangle}, \tag{6}$$

where t_0 and τ correspond to reference time and delay time, respectively, and $v_i(t)$ is the atomic velocity at time t. The average is carried over atoms of the same type and the reference time for the 10 ps period of data collection. Figure 11 presents the time dependence of the self-velocity autocorrelation function of the previously defined oxygen atom types O0, O1, and O2, which belong to the water molecules in the bulk state W0, with a single hydrogen bond formed with the COO^- group (W1), and with two hydrogen bonds formed with the COO^- groups (W2), respectively. The negative region of these oxygen VACF profiles implies that these molecules have a greater probability of rebounding within this time. In regard to bulk water, the O0 VACF shows a similar oscillation behavior to earlier simulation studies[51–53] and decays within approximately 0.6 ps. Whereas, due to attractive interactions associated with the COO^- groups, the O1 and O2 VACF profiles decay faster than the O0 about 0.38 and 0.25 ps, respectively. By integrating the O0, O1, and O2 VACF profiles, which are 8.1×10^{-3}, 7.8×10^{-4}, and 2.4×10^{-4} ps, respectively, we obtain a reasonable trend that shows the diffusion of water molecules slows down with stronger attractions from the COO^- groups.

Figure 12(a) presents the vibration spectra of the water oxygen types, O0, O1, and O2, which are obtained by applying the Fourier transformation to the VACF profiles. The O0

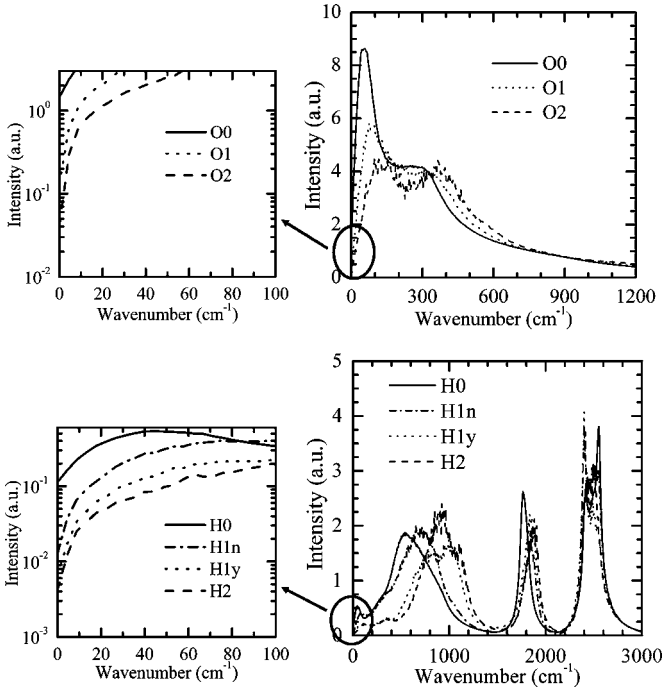

FIG. 12. Vibration spectra of (a) oxygen and (b) hydrogen atoms of water in different interaction states with the COO^- groups.

spectrum shows a major peak centered around 58 cm^{-1} and a broad shoulder peak at around 200–300 cm^{-1}, which has been observed in other MD studies.[50,54] When water molecules have stronger interactions with charged COO^- groups, through the formation of the hydrogen bonds (O2 > O1 > O0), we observe that both spectrum peaks shift to higher wave numbers. Worthy of note is that the second peak of the O2 spectrum (i.e., the bridged water molecules between two neighboring COO^- groups) moves significantly toward 400 cm^{-1}. Moreover, the second peak becomes more significant while the first peak shows an opposite trend. Similar to the low frequency Raman spectra of liquid water reported by Walrafen *et al.*,[55] these results imply that the second peak is primarily associated with the H-bonded O–O intermolecular stretching vibration, whereas the first peak is attributed to the non-H-bonded molecules. In Fig. 12(b) we present the hydrogen spectrum, which is typically related to the libration (400–1200 cm^{-1}), intramolecular bending (1200–2200 cm^{-1}), and intramolecular stretching (2200–4000 cm^{-1}) motions. It is apparent that the presence of the charged COO^- groups has a significant influence on the resulting hydrogen spectrum. To manifest this, we compare the positions of the three main peaks of the hydrogen spectra as shown in Table II. We find that for the H1y and H2 atoms, which are strongly connected to the oxygen atoms of the COO^- groups, both the libration and bending peaks shift significantly from a lower frequency for H0 towards a higher frequency, whereas the stretching peak shifts oppositely. For the H1n atoms, which are not directly adsorbed into the oxygen atoms of the COO^- groups, the shifting degrees of the main peak positions are not as significant as those obtained from the strongly bonded H1y and H2 atoms. Indeed, Marti *et al.*[50] also found similar trends, which they claimed are highly correlated to the formation of hydrogen bonds.

TABLE II. Positions of the three main peaks of hydrogen spectra.

	Libration (cm^{-1})	Bending (cm^{-1})	Stretching (cm^{-1})
H0	538	1773	2551
H1n	653	1836	2480
H1y	920	1836	2400
H2	924	1884	2400

IV. CONCLUSION

We employ all-atom molecular dynamics simulations to study a single molecule of PMAA at various charge densities f in aqueous solutions. We find that in addition to the repulsive electrostatic interactions between the charged COO^- groups, the local arrangement of water molecules surrounding the PMAA plays an important role in chain conformation behavior. The fact that the distance between the H atom of water and the charged O atom of the COO^- group is smaller than the normal hydrogen bonding length of 1.8 Å reveals very strong interactions between the COO^- and water. This indicates that water molecules are very likely to form shell-like layers surrounding the COO^- groups. In principle, each COO^- group is closely surrounded by three water molecules. Moreover, the water molecules often act as a bridging agent between two neighboring COO^- groups. Since bridged water molecules significantly limit torsional and bending degrees of the backbone monomers, it is reasonable to conclude that the rodlike chain conformation, exhibited by the strongly charged polymer chain, is significantly enhanced via the bridged water. When the charge density decreases, due to the number of less hydrophilic COOH groups, which prevent the absorption of water molecules surrounding the PMAA, along the chain increases, the chain forms a more coil-like conformation.

The strong attractive interaction between the charged COO^- group and water via the formation of hydrogen bonds holds great influence on both the PMAA chain conformation and the dynamic properties of water. This influence slows down water diffusion and enables the two characteristic peaks of the oxygen spectrum to shift to higher frequencies. When water molecules bridge between two neighboring COO^- groups, we observe a significant increase to the second peak of the corresponding oxygen spectrum ($\approx$100 cm^{-1}). This is not surprising since the second peak is mainly attributed to the H-bonded O–O intermolecular stretching vibration. In addition, the strong H-bonded interaction also causes a respective increase of 386 and 111 cm^{-1} to the libration and bending peaks of the hydrogen spectrum and a decrease of 151 cm^{-1} to the stretching peak.

ACKNOWLEDGMENT

This work was supported by the National Science Council of Taiwan, Republic of China under Grant Nos. NSC-94-2212-E-110-005, NSC-095-SAF-I-564-623-TMS, and NSC 95-2221-E-002-155.

[1] *Handbook of Polyelectrolytes and Their Applications*, edited by S. K. Tripathy, J. Kumar, and H. S. Nalwa (American Scientific, Stevenson Ranch, CA, 2002), Vol. 3.
[2] S. Hellebust, S. Nilsson, and A. M. Blokhus, Macromolecules **36**, 5372 (2003).
[3] M. Olvera de la Cruz, L. Belloni, M. Delsanti, J. P. Dalbiez, O. Spalla, and M. Drifford, J. Chem. Phys. **103**, 5781 (1995).
[4] F. Muller, P. Guenoun, M. Delsanti, B. Demé, L. Auvray, J. Yang, and J. W. Mays, Eur. Phys. J. E **15**, 465 (2004).
[5] R. D. Wesley, C. A. Dreiss, T. Cosgrove, S. P. Armes, L. Thompson, F. L. Baines, and N. C. Billingham, Langmuir **21**, 4856 (2005).
[6] P. Ravi, C. Wang, K. C. Tam, and L. H. Gan, Macromolecules **36**, 173 (2003).
[7] V. Sfica and C. Tsitsilianis, Macromolecules **36**, 4983 (2003).
[8] C. Wang, P. Ravi, K. C. Tam, and L. H. Gan, J. Phys. Chem. B **108**, 1621 (2004).
[9] H. Schiessel and P. Pincus, Macromolecules **21**, 7953 (1988).
[10] J. Wittner, A. Johner, and J. F. Joanny, J. Phys. II **5**, 635 (1995).
[11] P. Gonzalez-Mozuelos and M. Olvera de la Cruz, J. Chem. Phys. **103**, 3145 (1995).
[12] E. Raspaud, M. Olvera de la Cruz, J. L. Sikorav, and F. Livolant, Biophys. J. **74**, 381 (1998).
[13] N. V. Brilliantov, D. V. Kuznetsov, and R. Klein, Phys. Rev. Lett. **81**, 1433 (1998).
[14] E. Raspaud, I. Chaperon, A. Leforestier, and F. Livolant, Biophys. J. **77**, 1547 (1999).
[15] M. Muthukumar and G. Carri, J. Chem. Phys. **111**, 1765 (1999).
[16] T. T. Nguyen, I. Rouzina, and B. I. Shklovskii, J. Chem. Phys. **112**, 2562 (2000).
[17] F. J. Solis and M. Olvera de la Cruz, J. Chem. Phys. **112**, 2030 (2000).
[18] F. J. Solis and M. Olvera de la Cruz, Eur. Phys. J. E **4**, 143 (2001).
[19] F. J. Solis, J. Chem. Phys. **117**, 9009 (2002).
[20] P. Y. Hsiao and E. Luijten, Phys. Rev. Lett. **97**, 148301 (2006).
[21] M. J. Stevens and K. Kremer, J. Chem. Phys. **103**, 1669 (1995).
[22] M. J. Stevens and S. J. Plimpton, Eur. Phys. J. B **2**, 341 (1998).
[23] R. G. Winkler, M. Gold, and P. Reineker, Phys. Rev. Lett. **80**, 3731 (1998).
[24] U. Micka, C. Holm, and K. Kremer, Langmuir **15**, 4033 (1999).
[25] M. J. Stevens, Biophys. J. **80**, 130 (2001).
[26] R. G. Winkler, M. O. Steinhauser, and P. Reineker, Phys. Rev. E **66**, 021802 (2002).
[27] R. Messina, C. Holm, and K. Kremer, J. Chem. Phys. **117**, 2947 (2002).
[28] H. J. Limbach and C. Holm, J. Phys. Chem. B **107**, 8041 (2003).
[29] S. Liu, K. Ghosh, and M. Muthukumar, J. Chem. Phys. **119**, 1813 (2003).
[30] P. G. Khalatur, A. R. Khokhlov, D. A. Mologin, and P. Reineker, J. Chem. Phys. **119**, 1232 (2003).
[31] K. A. T. Silverstein, A. D. J. Haymet, and K. A. Dill, J. Am. Chem. Soc. **122**, 8037 (2000).
[32] S. Moelbert, B. Normand, and P. De Los Rios, Phys. Rev. E **69**, 061924 (2004).
[33] F. J. Solis, R. Weiss-Malik, and B. Vernon, Macromolecules **38**, 4456 (2005).
[34] D. A. C. Beck, D. O. V. Alonso, and V. Daggett, Biophys. Chem. **100**, 221 (2003).
[35] J. Dudowicz, K. F. Freed, and M. Y. Shen, J. Chem. Phys. **118**, 1989 (2003).
[36] S. S. Jang, V. Molinero, T. Cağin, and W. A. Goddard III, J. Phys. Chem. B **108**, 3149 (2004).
[37] S. S. Jang, S. T. Lin, T. Cağin, V. Molinero, and W. A. Goddard III, J. Phys. Chem. B **109**, 10154 (2005).
[38] S. T. Lin, P. K. Maiti, and W. A. Goddard III, J. Phys. Chem. B **109**, 8663 (2005).
[39] H. Morawetz and Y. Wang, Macromolecules **20**, 194 (1987).
[40] J. Zhang and N. A. Peppas, Macromolecules **33**, 102 (2000).
[41] S. V. Kazakov, V. I. Muronetz, M. B. Dainiak, V. A. Izumrudov, I. Y. Galaev, and B. Mattiasson, Macromol. Biosci. **1**, 157 (2001).
[42] P. Ravi, C. Wang, K. C. Tam, and L. H. Gan, Macromolecules **36**, 173 (2003).
[43] C. Wang, P. Ravi, K. C. Tam, and L. H. Gan, J. Phys. Chem. B **108**, 1621 (2004).
[44] J. Yao, P. Ravi, K. C. Tam, and L. H. Gan, Polymer **45**, 2781 (2004).
[45] M. Levitt, M. Hirshberg, R. Sharon, and V. Daggett, Comput. Phys. Commun. **91**, 215 (1995).
[46] M. Levitt, M. Hirshberg, R. Sharon, K. E. Laiding, and V. Daggett, J. Phys. Chem. B **101**, 5051 (1997).
[47] J. M. Haile, *Molecular Dynamics Simulation* (Wiley-Interscience, New York, 1992).
[48] D. C. Rapaport, *The Art of Molecular Dynamics Simulations* (Cambridge University Press, Cambridge, 1997).
[49] M. Praprotnik and D. Janežič, J. Chem. Phys. **122**, 174103 (2005).
[50] J. Martí, J. A. Padro, and E. Guárdia, J. Chem. Phys. **105**, 639 (1996).
[51] A. Chandra and T. Ichiye, J. Chem. Phys. **111**, 2701 (1999).
[52] N. Choudhury and B. M. Pettitt, J. Phys. Chem. B **109**, 6422 (2005).
[53] Z. Zhou, B. D. Todd, K. P. Travis, and R. J. Sadus, J. Chem. Phys. **123**, 054505 (2005).
[54] J. A. Padro, J. Marti, and E. Guardia, J. Phys.: Condens. Matter **6**, 2283 (1994).
[55] G. E. Walrafen, M. S. Hokmabadi, W. H. Yang, and Y. C. Chu, J. Phys. Chem. **93**, 2909 (1989).